



Published in final edited form as:

J Magn Reson Imaging. 2018 October ; 48(4): 1120–1128. doi:10.1002/jmri.26028.

The Variable Impact of CSF Flow Suppression on Quantitative 3.0T Intracranial Vessel Wall Measurements

Petrice M. Cogswell, MD, PhD¹, Jeroen C.W. Siero, PhD^{2,3}, Sarah K. Lants, BS¹, Spencer Waddle, BS¹, L. Taylor Davis, MD¹, Guillaume Gilbert, PhD⁴, Jeroen Hendrikse, MD², and Manus J. Donahue, PhD^{1,*}

¹Department of Radiology and Radiological Sciences, Vanderbilt University Medical Center, Nashville, TN, USA ²Department of Radiology, University Medical Center Utrecht, Utrecht, The Netherlands ³Spinoza Center for Neuroimaging, Amsterdam, The Netherlands ⁴MR Clinical Science, Philips Healthcare Canada, Markham, Ontario, Canada

Abstract

Background—Flow suppression techniques have been developed for intracranial (IC) vessel wall imaging (VWI) and optimized using simulations, however simulation results may not translate *in vivo*.

Purpose—To evaluate experimentally how IC vessel wall and lumen measurements change in identical subjects when evaluated using the most commonly-available blood and CSF flow suppression modules and VWI sequences.

Study type—Prospective.

Population/subjects—Healthy adults (n=13; age=37±15 years) were enrolled.

Field strength/sequence—A 3.0T 3D T_1 /proton density (PD)-weighted turbo-spin-echo (TSE) acquisition with post-readout anti-driven equilibrium module, with and without delay-alternating-with-nutation-for-tailored-excitation (DANTE) was applied. DANTE flip angle (8–12°) and TSE refocusing angle (sweep=40–120° or 50–120°) were varied.

Assessment—Basilar artery and internal carotid artery (ICA) wall thicknesses, CSF signal-to-noise ratio (SNR), contrast-to-noise ratio (CNR), and signal ratio (SR) were assessed. Measurements were made by two readers (radiology resident and board certified neuroradiologist).

Statistical tests—A Wilcoxon signed-rank test was applied with corrected two-sided $p < 0.05$ required for significance (critical p -value=0.008, 0.005, and 0.05 for SNR/CNR, SR, and wall thickness, respectively).

Results—A TSE pulse sweep=40–120° and sweep=50–120° provided similar ($p=0.55$) CSF suppression. Addition of the DANTE preparation reduced CSF SNR from 17.4 to 6.7, thereby providing significant ($p < 0.008$) improvement in CSF suppression. The DANTE preparation also resulted in a significant ($p < 0.008$) reduction in vessel wall SNR, but variable vessel wall to CSF

*Corresponding Author: Manus J. Donahue, PhD, Vanderbilt University Institute of Imaging Science, 1161 21st Avenue South, Nashville, TN 37232-2310, United States, mj.donahue@vanderbilt.edu, Tel:615.322.8350, Fax:615.322.0734.

CNR improvement ($p=0.87$). There was a trend for a difference in blood SNR with vs without DANTE ($p=0.05$). The wall thickness values were lower ($p<0.05$) with (basilar artery 4.45mm, 0.81mm, respectively) vs without (basilar artery 4.88mm, 0.97mm, respectively) DANTE 8°.

Data conclusion—IC VWI with TSE sweep=40–120° and with DANTE flip angle=8° provides the best CSF suppression and CNR of the approaches evaluated. However, improvements are heterogeneous, likely owing to inter-subject vessel pulsatility and CSF flow variations, which can lead to variable flow suppression efficacy in these velocity-dependent modules.

Keywords

vessel wall imaging; intracranial stenosis; DANTE; CSF

INTRODUCTION

Intracranial (IC) vessel wall imaging (VWI) at the clinical field strength of 3.0T has recently become available and is of growing interest to better characterize vessel wall thickening and plaque vulnerability in patients with IC vascular disease (1–6). To visualize vessel wall morphology, imaging must provide adequate suppression of intraluminal blood and surrounding cerebrospinal fluid (CSF) as well as maintain adequate signal-to-noise ratio (SNR) of the vessel wall and contrast-to-noise ratio (CNR) between the vessel wall and surrounding fluid.

Popular methods for arterial blood magnetization suppression utilize (i) a long, variable flip angle turbo-spin-echo readout (7, 8) which elicits intravoxel dephasing of flowing spins and (ii) inversion recovery or saturation recovery in which the repetition (TR) or inversion time (TI) are selected to maintain longitudinal blood magnetization near zero at the time of excitation. Basal cistern CSF signal surrounding major IC vessel wall segments may be suppressed using (i) inversion recovery preparations (9, 10) with TR and TI chosen to keep steady-state CSF magnetization near zero, (ii) post-readout anti-driven-equilibrium (ADE) modules (11, 12) which consist of a refocusing 180° radiofrequency (RF) pulse and a 90° RF pulse with an associated dephasing gradient, and/or (iii) Delay-Alternating-with-Nutation-for-Tailored-Excitation (DANTE) preparations (13–16), which use a series of low flip angle RF pulses with a pulsed field gradient to null signal from flowing spins such as blood and CSF.

These approaches have been evaluated separately and hold potential for IC VWI, however each have disadvantages. Inversion recovery methods are prone to SNR losses within the vessel wall, as low residual vessel wall magnetization is available at the TI required to null CSF at a field strength of 3.0T. ADE can reduce CSF signal, but is not effective for complete suppression. DANTE modules can increase CSF suppression further, but also reduce vessel wall SNR. Importantly, DANTE simulations have been performed (15), however simulations may not translate directly *in vivo* owing to motion from pulsation of the vessel wall and field inhomogeneities in CSF spaces such as the basal cisterns. A further complication is that CSF flow itself can be variable between subjects, and therefore it is unclear whether CSF suppression modules, which also frequently reduce vessel wall signal, are beneficial in all subjects.

The purpose of this work is to compare flow suppression and vessel wall measurements across multiple recently-developed 3.0T IC VWI techniques in identical subjects, outline standardized radiological procedures for measuring vessel lumen and wall thickness from these scans, and evaluate how common imaging metrics such as CNR, SNR, vessel lumen, and vessel wall thickness vary over a common range of parameter choices.

MATERIALS AND METHODS

Demographics

Healthy subjects (n=13; gender=4/9 male/female; age=37±15 years) provided informed, written consent for this HIPAA-compliant, IRB-approved study. Exclusion criteria included prior stroke, transient ischemic attack, heart attack, diabetes, BMI > 40, and arterial stenosis > 50%. One patient with prior left thalamic ischemic infarct and multifocal IC atherosclerotic disease was imaged to ensure that findings in healthy subjects translated to a patient with known vessel wall pathology.

3.0T vessel wall imaging pulse sequence

Table 1 shows the VWI pulse sequence variants that were investigated, which were motivated by promising variants from the literature (13). As we desired to reduce confounding from repositioning and compare different sequences directly, we required that all scans be performed in a single scan session of approximately one half hour and to enable clinical feasibility, in each scan we required a duration of approximately five minutes. For primary comparison, these included a 3D TSE readout with variable refocusing angle sweeps of (i) 40°–120° and (ii) 50°–120°, along with a 3D TSE readout with variable refocusing angle sweep of 40°–120° with DANTE flip angles of (iii) 8°, (iv) 10°, and (v) 12°. All approaches were required to have identical spatial resolution. As a secondary analysis, we also compared a T_2 -weighted approach, which required reduced slice coverage to maintain a clinically applicable acquisition time.

The TSE variable refocusing angle sweeps were chosen based on prior work using sweep of 50°–120° (7) and showing that a lower minimal flip angle may result in improved flow suppression (17). The maximal flip angle was held constant at 120° as flip angles greater than this largely increase the specific absorption rate (SAR) with minimal increases in SNR. To provide a longer duration signal with less decay, the variable flip angle sweeps were optimized for vessel wall signal preservation and have a half-exponential profile rather than a linear profile as used in prior work (7).

For DANTE, the flip angle was varied only as it was previously shown to have the greatest effect on flow suppression (13). The effect of TR on signal evolution was not evaluated as the TR effect is reduced by the anti-driven equilibrium module, and longer TRs render the sequence clinically impractical.

Simulations

Magnetization was simulated over the DANTE module for CSF ($T_1=4300$ ms, $T_2=1442$ ms, velocity=2 cm/s) and arterial IC blood ($T_1=1700$ ms, $T_2=120$ ms, velocity=40 cm/s) (18).

Flowing spins lose signal due to quadratic phase accumulation over the transient steady state, while signal is relatively preserved in static tissues driven to steady state. The effect of the DANTE flip angle and number of repetitions on longitudinal signal evolution has been investigated (13, 15) and here Bloch equation simulations were performed to evaluate the effects of different DANTE flip angles on the CSF, vessel wall, and blood signal.

Imaging experiments

Scans (Table 1) were performed on a 3.0T whole body scanner (Philips Achieva, Philips Healthcare, Best, The Netherlands) using body coil transmission and a 32-channel receive head coil. The base T_1 -/ PD -weighted 3D-TSE acquisition had an axial orientation with TSE-factor=56, TR/TE=1500/33 ms, field-of-view(FOV)= $200 \times 166 \times 45$ mm³, in-plane spatial resolution= 0.5×0.5 mm², SENSE factor=2, slice thickness=1 mm, duration=4min42 s and was applied with variable refocusing angle sweep= 40° – 120° and sweep= 50° – 120° . DANTE parameters for the subset of scans which used this module were repetitions=300, interval=1.1 ms, gradient strength in three directions=22.5 mT/m, and flip angle= 8° , 10° , or 12° . Finally, a T_2 -weighted scan with a 3D-TSE readout (TSE-factor=15, TR/TE=4000/83 ms, FOV= $200 \times 166 \times 21.6$ mm³, in-plane spatial resolution= 0.5×0.5 mm², SENSE factor=2, slice thickness=2.4 mm, duration=5min12 s) with variable refocusing angle sweep= 40° – 120° and DANTE flip angle 10° was evaluated as a secondary comparison. The T_2 -weighted sequence required a greater slice thickness and reduced slice coverage to maintain a clinically-applicable imaging time.

Analysis

Analysis was performed jointly by a radiology resident (three years of experience) and board-certified neuroradiologist (eight years of experience) using OsiriX (Pixmeo, Bernex, Switzerland). First, all scans were assessed visually and qualitatively to determine if the vessel wall was discernable at the measurement locations. SNR of the CSF, blood, vessel wall, and brain parenchyma was calculated as the mean signal within a region of interest (ROI) divided by standard deviation of the noise, taking into account the Rician noise distribution. The CNR of the vessel wall to CSF and vessel wall to blood was calculated as the difference in mean signal divided by the standard deviation of the thermal noise. The signal ratio (SR) of the vessel wall to the CSF and vessel wall to the blood were calculated as the ratio of the mean signal in the vessel wall ROI and CSF or blood ROIs.

The CSF signal was measured in the prepontine cistern, the blood signal in the basilar artery lumen, and the parenchyma signal in the central pons. Vessel wall ROIs were drawn for each acquisition to outline the inner and outer borders of the basilar artery in a single slice between the anterior inferior cerebellar artery (AICA) and superior cerebellar artery (SCA).

Vessel wall thickness measurements were made in the anatomic left-right direction in a plane orthogonal to the vessel length using OsiriX multi-planar reformatting tool (Figure 2). This procedure ensures that the vessel lumen and wall measurement are not performed obliquely across the vessel, which would lead to more variable measurements that depended sensitively on head positioning and slice planning. The supraclinoid internal carotid arteries

(ICAs) and the basilar artery, between the AICA and SCA, were evaluated. Wall thickness was calculated as half the difference of the outer wall and luminal diameters.

Statistical considerations

Evaluation proceeded in a step-wise fashion, first evaluating which methods had the best SNR and CNR, and subsequently comparing vessel wall measurements in the best candidate sequences with and without the DANTE module. A Wilcoxon signed-rank test was used for comparison of all study parameters across different scan sequences, a critical two-sided p -value < 0.05 was required for significance, and p -values were interpreted in the context of Bonferroni multiple comparisons correction where applicable. Note that as the data analysis was step-wise, different comparisons have different critical p -values, as outlined below.

First, separate SNR (vessel wall and CSF), CNR (vessel wall to CSF and vessel wall to blood), and SR (vessel wall to CSF and vessel wall to blood) measurements were compared between the scans without DANTE for the sweep= 40° – 120° and sweep= 50° – 120° acquisitions. The purpose of this initial comparison was to determine how the TSE sweep influenced these parameters in the absence of DANTE, and to provide a base sequence for comparison with the addition of the DANTE preparations. Here, for each observable one comparison was made between each of the two sequences and the p -value required for significance of was $p < 0.05$.

Second, separate SNR and CNR measurements were compared among the above-determined base sequence (see Results; sweep= 40° – 120° without DANTE) and the (i) DANTE 8° , (ii) DANTE 10° , and (iii) DANTE 12° acquisitions with the same readout. The purpose of this comparison was to understand how addition of the DANTE module influenced the SNR and CNR measurements when identical TSE readouts were used. For each observable (SNR or CNR), a total of six separate comparisons were made and therefore a two-sided critical $p < 0.008$ was required for significance. The T_2 -weighted acquisition was not included in these comparisons due to the difference in slice thickness and FOV.

The SR of the vessel wall to CSF and vessel wall to blood were compared among the base sequence (sweep= 40° – 120°) without DANTE and the DANTE 8° , DANTE 10° , DANTE 12° , and T_2 -weighted DANTE 10° acquisitions with the same TSE readouts. The purpose of this comparison was to understand how addition of the DANTE module influenced the SR when TSE readouts with identical refocusing sweeps were used. A total of 10 comparisons were made, giving a two-sided Bonferroni-corrected $p < 0.005$ required for significance.

From these initial comparisons, it was determined how the addition of DANTE affected SNR, CNR, and SR. To determine the impact of DANTE on the vessel wall measurement, a Wilcoxon signed-rank test was used to evaluate differences in vessel wall measurements between the 3D-TSE base sequence without DANTE sweep= 40° – 120° and the DANTE 8° sequence with an identical 3D TSE readout and pulse sweep= 40° – 120° ; this comparison of the two best sequences was determined by the above results of the best two candidate sequences (see Results). The outer wall diameter, luminal diameter, and wall thickness were compared between the two acquisitions, separately for the basilar artery, supraclinoid right ICA, and supraclinoid left ICA ($p < 0.05$).

RESULTS

Simulations

Figure 1B, C shows the evolution of the magnetization over the DANTE preparation module. Blood magnetization was largely suppressed in both cases, however CSF magnetization was more variable owing to the longer T_2 and slower flow velocity, and the impact of CSF suppression was evaluated experimentally here. The point-spread-function of the 3D TSE readout is approximately 1.1 voxels. Note that velocity and relaxation time parameters for CSF and blood are approximate and taken from literature, however these may vary between subjects and lead to subject-specific flow suppression performance, which was evaluated here.

Imaging

Representative images from each acquisition (Table 1) in two subjects are shown in Figure 3. Improved CSF suppression was visually appreciable in the basilar cistern with DANTE in most subjects, albeit with decreased wall signal. However, a subgroup of subjects (3/13) showed low CSF signal in the basal cisterns without DANTE and therefore little further reduction in CSF signal with the DANTE module. Results from a 53-year-old female patient with multifocal intracranial atherosclerosis and prior left thalamic infarct (Figure 3) demonstrate a region of hyperintense wall signal and thickening of the basilar artery that is better seen with the use of the DANTE preparation. SNR, CNR, and SR analysis on this patient were consistent with group-level findings from healthy subjects.

Figures 4 and 5 summarize the group SNR, CNR, and SR results. Two of the T_2 -weighted scans and one of the DANTE scans were of insufficient quality for assessment. There was no significant difference between the no DANTE sweep= 40° – 120° and sweep= 50° – 120° acquisitions for any of the comparisons on average ($p>0.55$).

The addition of the DANTE preparation provided significant improvement in CSF suppression (SNR measurement; $p<0.008$) when comparing the no DANTE protocol with each of the DANTE 8° , 10° and 12° acquisitions. The DANTE preparation also resulted in a significant reduction ($p<0.008$) in vessel wall SNR and a trend toward improvement in the SR ($p=0.06$; no DANTE vs DANTE 8°). The majority of subjects (10/13) showed improved CNR of the vessel wall to CSF with DANTE, however, group trends are not significant due to a decrease in CNR of the vessel wall to CSF with DANTE in the three subjects who showed good CSF suppression without DANTE. CSF suppression improved ($p<0.008$) from DANTE flip angle 8° to DANTE 10° and 12° but not between DANTE 10° and 12° . Vessel wall SNR was reduced with DANTE flip angle 12° compared to 8° ($p<0.008$), but was not significantly different between DANTE 8° to 10° and 10° to 12° . The background noise was not significantly different between any of the acquisitions.

There was a strong trend for a decrease in the SNR of blood between the DANTE 8° , sweep= 40 – 120° and the base (without DANTE) sweep= 40 – 120° acquisition ($p=0.05$). The SR and CNR of the vessel wall to blood decreased with the addition of the DANTE module ($p<0.005$ and $p<0.008$, respectively).

The T_2 -weighted acquisition with pulse sweep=40°–120° and DANTE flip angle 10° demonstrated no significant difference in SR of the vessel wall to the CSF versus the comparable proton density-weighted acquisition ($p=0.20$).

The comparison of vessel wall thickness measurements with and without DANTE is summarized in Figure 6. The outer vessel wall diameter and wall thickness were significantly less with vs without DANTE ($p<0.05$) for the left ICA and basilar artery.

DISCUSSION

We compared variable flip angle TSE readouts and flow suppression techniques, including variations of the DANTE preparation in a group of healthy subjects. Addition of the DANTE module resulted in improved flow suppression as well as loss of vessel wall signal that is minimized with low DANTE flip angles on average. In approximately a quarter of subjects, the CSF signal was sufficiently low with the 3D TSE readout alone that the addition of DANTE served primarily to reduce the vessel wall signal. The CSF suppression was visually improved in some subjects but not significantly improved on average with sweep=40°–120° versus sweep=50°–120°, in both the simulations and *in vivo* studies, which corresponds with prior work showing that a lower initial flip angle offers better flow suppression (17). The sweep=40°–120° acquisition is expected to provide slightly lower SNR than the sweep=50°–120° due the smaller flip angle applied when sampling the center of k -space, while providing better sharpness due to an improved point spread function, though no qualitative difference was detectable for either of these parameters.

With the improved CSF suppression provided by DANTE, the vessel wall was often better delineated, however in some subjects visualization of the full circumference of the vessel wall was difficult or the wall signal appeared mottled. The decreased wall signal with DANTE is likely in part due to the pulsation of the vessel wall, affected by the motion sensitive DANTE pulse (15). As shown in prior simulations (13), a larger DANTE flip angle resulted in greater suppression of signal in both the CSF and static tissues (vessel wall and parenchyma), though the difference was greater in the CSF as suggested by an increase in SR of the vessel wall to CSF with greater DANTE flip angles. Through both quantitative and qualitative evaluation of the experimental DANTE results, the DANTE preparation with a flip angle of 8° may be a reasonable compromise to minimize static SNR losses that may degrade vessel wall depiction, while achieving improved CSF suppression. These findings suggest that while DANTE should be considered in many subjects to improve CSF suppression, improvements may be required in subjects with low CSF flow to reduce vessel wall SNR reductions. Novel research avenues may focus on utilizing DANTE principles to quantify vessel pulsatility or basal cistern CSF flow velocity and composition, which may even provide a more comprehensive perspective on disease status than from vessel morphology alone.

While CSF suppression was often improved with DANTE, blood suppression was not significantly changed and therefore DANTE may not be required for additional blood suppression when TSE readouts are used. The T_2 -weighted acquisition with sweep=40°–120°, DANTE flip angle of 10° provided comparable SNR of the vessel wall to that of the

corresponding T_1 - PD -weighted acquisition, when accounting for the difference in FOV and slice thickness.

The outer wall diameter and therefore wall thickness were significantly reduced with the application of DANTE for the basilar artery and left supraclinoid ICA. This is likely secondary to inadequate CSF suppression confounding the vessel wall border in acquisitions without DANTE in some subjects. The lack of significant difference in the outer diameter of the right ICA may be due to limited statistical power. The luminal diameters were not significantly different with vs without DANTE, again suggesting relatively good suppression of blood signal with the TSE readout. Wall thicknesses of approximately 1.0–1.1 mm for the ICAs and 0.8–1.0 mm for the basilar artery are similar to previously reported mean ICA wall thickness of 1.0 mm and maximum basilar artery wall thickness of 0.8–0.9 mm (7).

Several limitations should be considered. First, the DANTE flip angles were varied only as this was previously shown to have the largest effect on CSF suppression (13), while other factors such as the gradient strength and spacing were chosen based on prior experimental work and simulations. Second, non-DANTE parameters such as the spatial resolution were fixed and the acquired spatial resolution was isotropic in-plane only, which may impair evaluation of tortuous vessels. Third, we targeted larger intracranial vessels for measurement, but in the future higher achievable spatial resolution would allow for more accurate evaluation of the more distal intracranial vasculature. Fourth, a relatively small number of subjects and only one patient were included in this technical study. Finally, a T_1 - PD -weighted acquisition was chosen for experimental evaluation or variations of the DANTE preparation, as vessel wall conspicuity has been shown to be comparable among various weightings these results are anticipated to be similar (19).

In conclusion, a VWI acquisition with a 3D-TSE readout refocusing pulse sweep=40°–120° and DANTE preparation with flip angle 8° provides the best CSF suppression on average and maintenance of vessel wall signal of the evaluated techniques. However, it should also be noted that CSF suppression using these parameters can be variable and reduces vessel wall signal, and personalized sequences that incorporate CSF flow velocity measurements or more complex suppression techniques should be pursued.

Acknowledgments

Grant funding: NIH/NINDS 1R01NS07882801A1, NIH/NINDS 1R01NS097763, NIH/NINR 1R01NR01507901, AHA Southeastern affiliate 14GRNT20150004, AHA National affiliate 14CSA20380466.

References

1. Mandell DM, Mossa-Basha M, Qiao Y, et al. Intracranial Vessel Wall MRI: Principles and Expert Consensus Recommendations of the American Society of Neuroradiology. *Am J Neuroradiol*. 2016
2. Lam WWM, Wong KS, So NMC, Yeung TK, Gao S. Plaque Volume Measurement by Magnetic Resonance Imaging as an Index of Remodeling of Middle Cerebral Artery: Correlation with Transcranial Color Doppler and Magnetic Resonance Angiography. *Cerebrovasc Dis*. 2004; 17:166–169. [PubMed: 14707417]
3. Xu W-H, Li M-L, Gao S, et al. In vivo high-resolution MR imaging of symptomatic and asymptomatic middle cerebral artery atherosclerotic stenosis. *Atherosclerosis*. 2010; 212:507–511. [PubMed: 20638663]

4. Chung GH, Kwak HS, Hwang SB, Jin GY. High resolution MR imaging in patients with symptomatic middle cerebral artery stenosis. *Eur J Radiol.* 2012; 81:4069–4074. [PubMed: 22846476]
5. Mossa-Basha M, Hwang WD, De Havenon A, et al. Multicontrast high-resolution vessel wall magnetic resonance imaging and its value in differentiating intracranial vasculopathic processes. *Stroke J Cereb Circ.* 2015; 46:1567–1573.
6. Dieleman N, Yang W, van der Kolk AG, et al. Qualitative Evaluation of a High-Resolution 3D Multi-Sequence Intracranial Vessel Wall Protocol at 3 Tesla MRI. *PLOS ONE.* 2016; 11:e0160781. [PubMed: 27532106]
7. Qiao Y, Steinman DA, Qin Q, et al. Intracranial arterial wall imaging using three-dimensional high isotropic resolution black blood MRI at 3.0 Tesla. *J Magn Reson Imaging JMRI.* 2011; 34:22–30. [PubMed: 21698704]
8. Hennig J, Weigel M, Scheffler K. Multiecho sequences with variable refocusing flip angles: optimization of signal behavior using smooth transitions between pseudo steady states (TRAPS). *Magn Reson Med.* 2003; 49:527–535. [PubMed: 12594756]
9. van der Kolk AG, Zwanenburg JJM, Brundel M, et al. Intracranial Vessel Wall Imaging at 7.0-T MRI. *Stroke.* 2011; 42:2478–2484. [PubMed: 21757674]
10. Fan Z, Yang Q, Deng Z, et al. Whole-brain intracranial vessel wall imaging at 3 Tesla using cerebrospinal fluid-attenuated T1-weighted 3D turbo spin echo. *Magn Reson Med.* 2017; 77:1142–1150. [PubMed: 26923198]
11. Yang H, Zhang X, Qin Q, Liu L, Wasserman BA, Qiao Y. Improved cerebrospinal fluid suppression for intracranial vessel wall MRI. *J Magn Reson Imaging JMRI.* 2016; 44:665–672. [PubMed: 26950926]
12. Dieleman N, Yang W, Abrigo JM, et al. Magnetic Resonance Imaging of Plaque Morphology, Burden, and Distribution in Patients With Symptomatic Middle Cerebral Artery Stenosis. *Stroke.* 2016; 47:1797–1802. [PubMed: 27301944]
13. Li L, Miller KL, Jezzard P. DANTE-prepared pulse trains: a novel approach to motion-sensitized and motion-suppressed quantitative magnetic resonance imaging. *Magn Reson Med.* 2012; 68:1423–1438. [PubMed: 22246917]
14. Wang J, Helle M, Zhou Z, Börnert P, Hatsukami TS, Yuan C. Joint blood and cerebrospinal fluid suppression for intracranial vessel wall MRI. *Magn Reson Med.* 2016; 75:831–838. [PubMed: 25772551]
15. Viessmann O, Li L, Benjamin P, Jezzard P. T2-Weighted intracranial vessel wall imaging at 7 Tesla using a DANTE-prepared variable flip angle turbo spin echo readout (DANTE-SPACE). *Magn Reson Med.* 2016
16. Zhang L, Zhang N, Wu J, Liu X, Chung Y-C. High resolution simultaneous imaging of intracranial and extracranial arterial wall with improved cerebrospinal fluid suppression. *Magn Reson Imaging.* 2017; 44:65–71. [PubMed: 28807750]
17. ISMRM. Flow Sensitivity of CPMG Sequences with Variable Flip Refocusing and Implications for CSF Signal Uniformity in 3D-FSE Imaging. 2006. [<http://dev.ismrm.org/2006/2430.html>]
18. Enzmann DR, Ross MR, Marks MP, Pelc NJ. Blood flow in major cerebral arteries measured by phase-contrast cine MR. *Am J Neuroradiol.* 1994; 15:123–129. [PubMed: 8141043]
19. van der Kolk AG, Hendrikse J, Brundel M, et al. Multi-sequence whole-brain intracranial vessel wall imaging at 7.0 tesla. *Eur Radiol.* 2013; 23:2996–3004. [PubMed: 23736375]

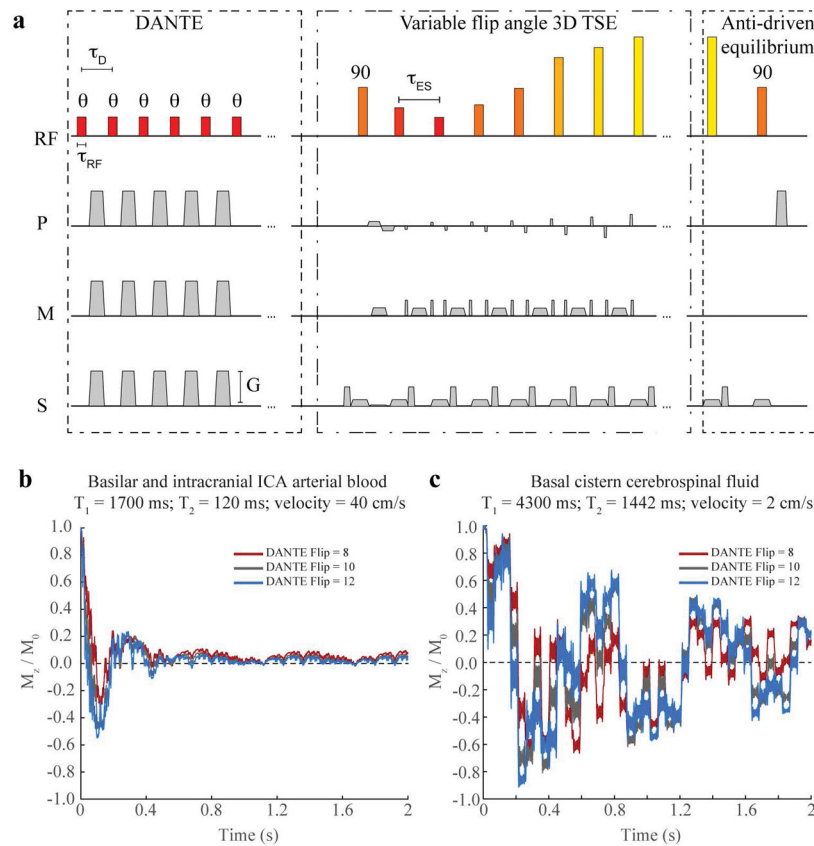


Figure 1.

The vessel wall imaging pulse sequence (a), which consists of a low-flip-angle delay alternating nutation with tailored excitation (DANTE) module, followed by a variable refocusing angle 3D turbo-spin-echo (TSE) readout, and concludes with an anti-driven equilibrium module to reduce steady-state cerebrospinal signal magnetization. Block pulses are shown for simplicity, however only the DANTE pulses are block pulses, TSE refocusing pulses are sinc-gauss pulses (five lobes; duration=5.9 ms), and the anti-driven equilibrium pulse is an asymmetric sinc-gauss pulse (seven lobes; duration=4.4 ms). Below, longitudinal magnetization is simulated for the DANTE pulse train for blood (b) and CSF (c) for physiological intracranial blood flow velocities or basal cistern CSF velocities. Blood magnetization converges to zero, however the CSF magnetization is more variable, and suppression is evaluated experimentally in this study.

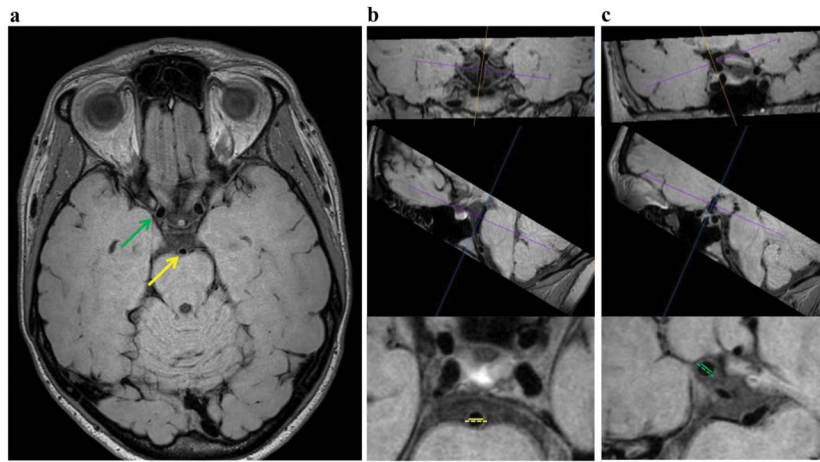


Figure 2. Representative full FOV slice in the acquired plane (a) and example wall thickness measurements performed in a plane perpendicular to vessel course using a multi-planar reformatting tool (b,c). The basilar artery (yellow) wall thickness measured between the AICA and SCA (b) and supraclinoid ICA (green) wall thickness measurements (c) are demonstrated. The dashed lines represent the outer vessel wall diameter and the solid lines the luminal diameter.

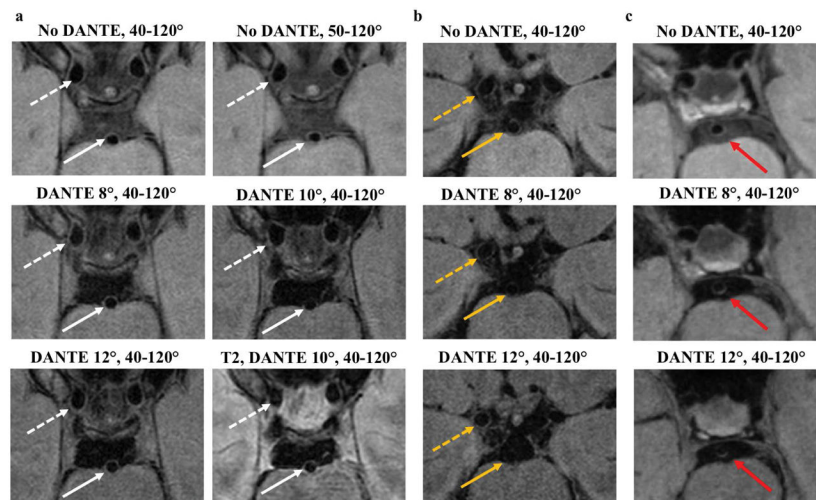


Figure 3. Examples of the CSF suppression techniques in two subjects and one patient. Cropped views from a single slice in the acquired plane from the first subject (a) show improved CSF suppression in the prepontine cistern with DANTE. The walls of the basilar artery (white arrow) and supraclinoid internal carotid arteries (white dashed arrow) are well-depicted. A second subject (b) shows relatively good CSF suppression with the 3D TSE readout without DANTE (no DANTE, 40–120°) and therefore little further decrease in CSF signal with DANTE. In this subject, the DANTE 12° acquisition resulted in signal loss of the basilar artery vessel wall (dashed yellow arrow), making it hard to discern the wall throughout its circumference. The right ICA vessel wall (yellow arrow) remains well visualized with DANTE. Patient example (c) of 53-year-old female with multifocal intracranial atherosclerosis and prior left thalamic ischemic infarct. Hyperintense basilar artery wall lesion (red arrow) is more conspicuous with the addition of DANTE.

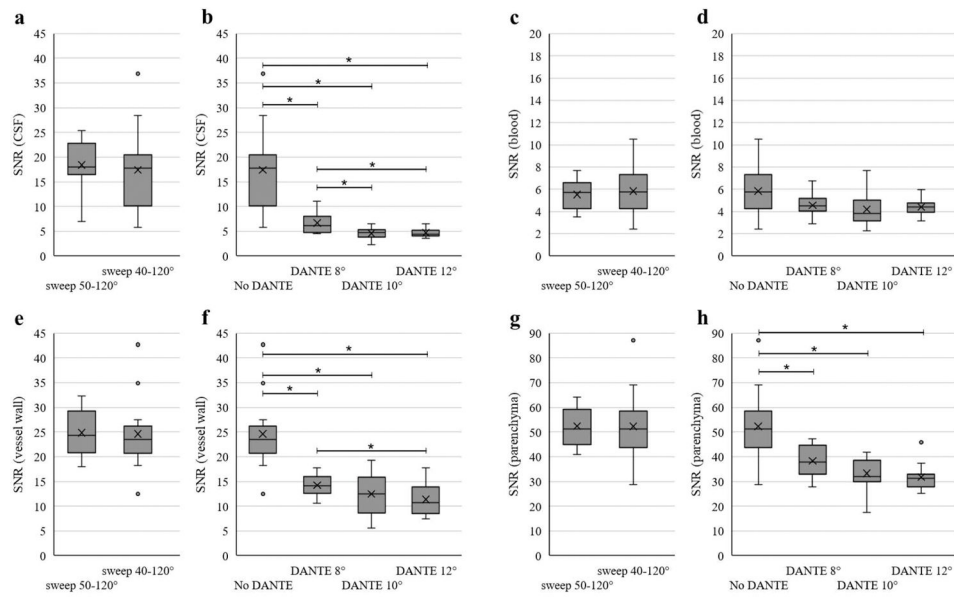


Figure 4.

Box plots show mean (X) and distribution of data points for SNR of the CSF (a, b), SNR of the blood (c, d), SNR of the vessel wall measured in the basilar artery (e, f), and SNR of the parenchyma measured in the pons (g, h). The central line represents the median, the X the mean, the lower and upper margins of the box the 25–75th percentile, and the whiskers all data excluding outliers. The vertical axis scale is different for the blood and parenchyma plots compared to the other SNR plots to better show the distribution of data. Statistical comparisons were performed separately for the no DANTE sweep 50°–120° versus sweep 40°–120° acquisitions (a, c, e, g) and then among the no DANTE sweep 40°–120° and the DANTE acquisitions (b, d, f, h). No significant difference was found between the no DANTE sweep 50°–120° versus sweep 40°–120° for any of the measures ($p < 0.05$). * indicates significance with multiple comparisons ($p < 0.008$) for the no DANTE vs DANTE comparisons.

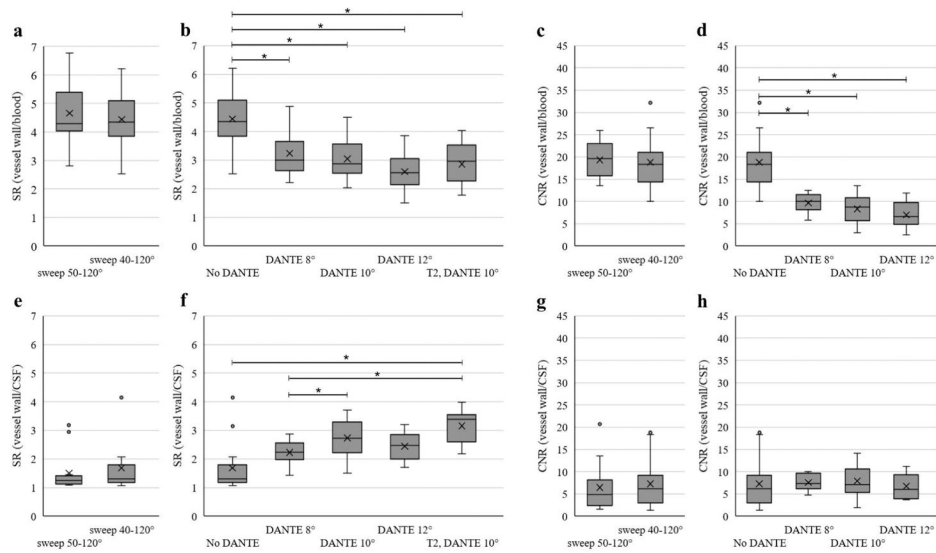


Figure 5.

Box plots show signal ratio (SR) of the vessel wall to blood (a, b), CNR of vessel wall to blood (c, d), SR of vessel wall to blood (e, f), and CNR of the vessel wall to CSF (g, h). The central line represents the median, \bar{X} the mean, the lower and upper margins of the box the 25–75th percentile, and the whiskers all data excluding outliers. The comparison of no DANTE sweep 50°–120° versus sweep 40°–120° acquisition (a, c, e, g) and among the no DANTE sweep 40°–120° and the DANTE acquisitions (b, d, f, h) are shown separately for each measure. No significant difference was found between the no DANTE sweep 50°–120° versus sweep 40°–120° acquisitions for any of the comparisons ($p < 0.05$). For the comparisons among the no DANTE sweep 40°–120° and the DANTE acquisitions, * indicates significance with multiple comparisons ($p < 0.008$ for CNR and $p < 0.005$ for SR, as T2-weighted scan was included for the SR analysis).

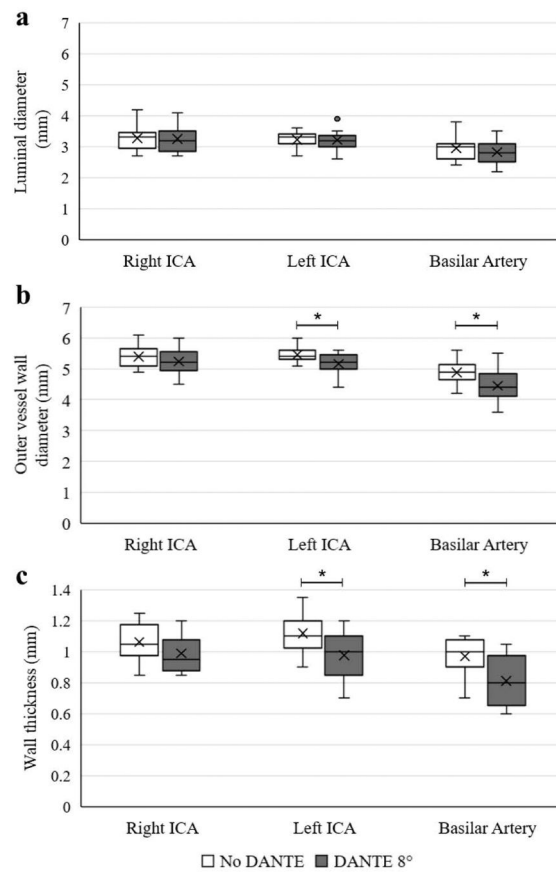


Figure 6.

Results of vessel wall measurements are shown by box plots of the luminal diameter (a), outer vessel wall diameter (b), and wall thickness (c) for the right ICA, left ICA, and basilar artery comparing the no DANTE, pulse sweep 40°–120° and the DANTE 8°, pulse sweep 40°–120° acquisitions. The central line represents the median, *X* the mean, the lower and upper margins of the box the 25–75th percentile, and the whiskers all data excluding outliers. *statistical significance with $p < 0.05$.

Table 1

Imaging protocol and acquisition parameters.

Imaging Sequence	TR (ms)	TE (ms)	DANTE flip angle	Refocusing pulse train	FOV (mm ³)	Spatial resolution (mm ³)	Time (min:s)
<i>Base 3D TSE VWI</i>							
sweep 40–120°	1500	33	-	40°–120°	200×166×45	0.5×0.5×1.0	4:42
sweep 50–120°	1500	33	-	50°–120°	200×166×45	0.5×0.5×1.0	4:42
<i>3D TSE VWI with DANTE</i>							
DANTE 8°	1500	33	8°	40°–120°	200×166×45	0.5×0.5×1.0	4:42
DANTE 10°	1500	33	10°	40°–120°	200×166×45	0.5×0.5×1.0	4:42
DANTE 12°	1500	33	12°	40°–120°	200×166×45	0.5×0.5×1.0	4:42
<i>VWI scan (for secondary analysis)</i>							
T2-weighted	4000	83	10°	40°–120°	200×166×21.6	0.5×0.5×2.4	5:12